E. 2008 Experiment

E-1. Overview of the 2008 experiment

The WWRP B08RDP experiment in 2008 was conducted one month from 24 July to 24 August 2008, in conjunction with the Beijing Olympic Games (8-24 August 2008). As in the 2007 experiment, 6 centers (MRI/JMA, NCEP, MSC, ZAMG, NMC/CMA and CAMS/CMA) participated in the Tier-1 mesoscale ensemble prediction. Specifications of Tier-1 ensemble prediction system of 6 participants in 2008 are listed in Table E-1-1.

Table E-1-1. Specifications of Tier-1 EPS of six participating centers in the 2008 experiment.

Participants	Model	IC	IC perturbation	LBC	LBC perturbation	Physical perturbation
NCEP*	WRF-ARW (L60M5) WRF-NMM (L60M5) GEFS (T284L60M5)	NCEP Global 3DVAR	Breeding	NCEP Global EPS	NCEP Global EPS	Multi-model
MRI/JMA	JMA-NHM (L40M11)	Meso 4DVAR	Targeted Global SV	JMA GSM Forecast	GSM forecast from targeted SV	non
MSC	GEM (L28M20)	MSC Global EnKF	MSC Global EnKF	MSC Global EPS	MSC Global EPS	Physical tendency perturbation with Markov chain, surface perturbation
ZAMG & Meteo-Fr.	ALANDIN (L37M17)	ECMWF Global 4DVAR	Blending ECMWF SV with ALADIN Bred Mode	ECMWF Global EPS	ECMWF Global EPS	Multi-physics
NMC/CMA	WRF-ARW (L31M15)	WRF-3DVAR	Breeding	CMA Global EPS	Global EPS	Multi-physics
CAMS/CMA	GRAPES (L31M9)	GRAPES-3DVAR	Breeding	CMA Global EPS	Global EPS	Multi-physics

To ameliorate the deficits found in the 2007 experiment, convective parameterization, surface process and the numerical diffusion in MRI/JMA's EPS were revised (E-2). To prepare initial conditions of the control run, Meso 4D-VAR was applied to the Beijing area (E-3-1). As for the initial perturbation method, global targeted singular vector method (E-4-2) was adopted, while five perturbation methods (E-4-1, 2, 3, 4 and 5) were developed or modified and compared in advance (E-4-6).

Lateral boundary conditions were given by JMA's operational high resolution GSM (E-3-5), while boundary perturbation methods were newly developed (E-5).

Specifications of the 2007 EPS system of MRI/JMA are listed in Table. E-2-1, compared with specifications of the 2006 and 2007 experiments.

E-2. Numerical model for the 2008 experiment

Specifications of the 2008 EPS of MRI/JMA are listed in Table. E-2-1, compared with specifications of the 2006 and 2007 experiments. In 2008, a version of NHM as of July 2008 was employed as for the forecast model, where radiation process was revised (Nagasawa, 2009). To ameliorate underestimations of convective rains and maximum temperatures in abnormally hot days found in the 2007 experiment (see, D-7-1), convective parameterization and surface process were modified. The generalized vertical hybrid coordinates, which were not employed in the 2007 experiment, were adopted in the forecast model and initial/lateral perturbations.

Table E-2-1. Specifications of the B08RDP MEP system of MRI/JMA.

	2006 Experiment	2007 Experiment	2008 Experiment
Forecast model	NHM as of March 2006	NHM as of May 2007	NHM as of July 2008
Horizontal grid	221×201 (Δx = 15km)	232×200 (Δx = 15km),	No change
Vertical grid	Terrain-following coordinates, 40 levels	No changes	Generalized hybrid coordinates
Number of members	11 members	No changes	No changes
Initial condition	Initial condition of RSM produced by JMA operational regional 4D-Var (20 km resolution)	JMA operational regional 4D-Var (20 km resolution)	Meso 4DVAR analysis for Beijing area
Initial perturbation	JMA one-week global EPS (TL159)	Targeted moist global SV (T63L40)	Targeted moist global SV (T63L40) (modified)
Lateral boundary	JMA RSM forecast (20km L40)	No changes	JMA GSM forecast (20km L60)
Lateral boundary perturbation	No	No	Forecast of GSM (T63L40) perturbed by GSV
Soil temperatures	4 layer prognostic soil temperatures	Initial perturbations are added	No changes

E-2-1. Tuning of the Kain-Fritsch parameterization

Underestimation of convective rains was found in the 2007 experiment (D-7-1). One of the causes of this underestimation was that parameters of the K-F convective parameterization scheme used in the 2007 experiment were the same as in the JMA's operational model setting for the 5 km horizontal resolution. Some of parameters in the JMA operational forecast were changed when the horizontal resolution of MSM was enhanced from 10 km to 5km in March 2006. Prior to the 2008 experiment, we tested following parameters to optimize the K-F scheme for the 15 km horizontal resolution.

- cu_lifetime_min: Life time for deep convection
- shallow_lifetime: Life time for shallow convection
- kf_thresh: Auto-conversion threshold from condensed water to rain

In the 2007 experiment, cu_lifetime_min was 900 s, shallow_lifetime was 600s and kf_thresh was 2 g/Kg according to the operational parameter setting of MSM with a horizontal resolution of 5 km. In the 2008 experiment, we changed above parameters to the setting of the 10km MSM

(cu_lifetime_min=1800 s, shallow_lifetime=2400 s, kf_thresh=0.8 g/Kg) and additionally tested a smaller value of kf_thresh (0.6 g/Kg).

Figure E-2-1 shows the accumulated 3 hour precipitation with the 15 km NHM for 21 UTC 1 August 2007. In this case, strong convective precipitation was observed south of Beijing (Fig. E-2-1a). In the 2007 experimental setting, NHM predicted a precipitation area at south of Beijing but the intensity was weak (Fig. E-2-1b). Using the new parameter setting, the rainfall rate increased (Fig. E-2-1c).

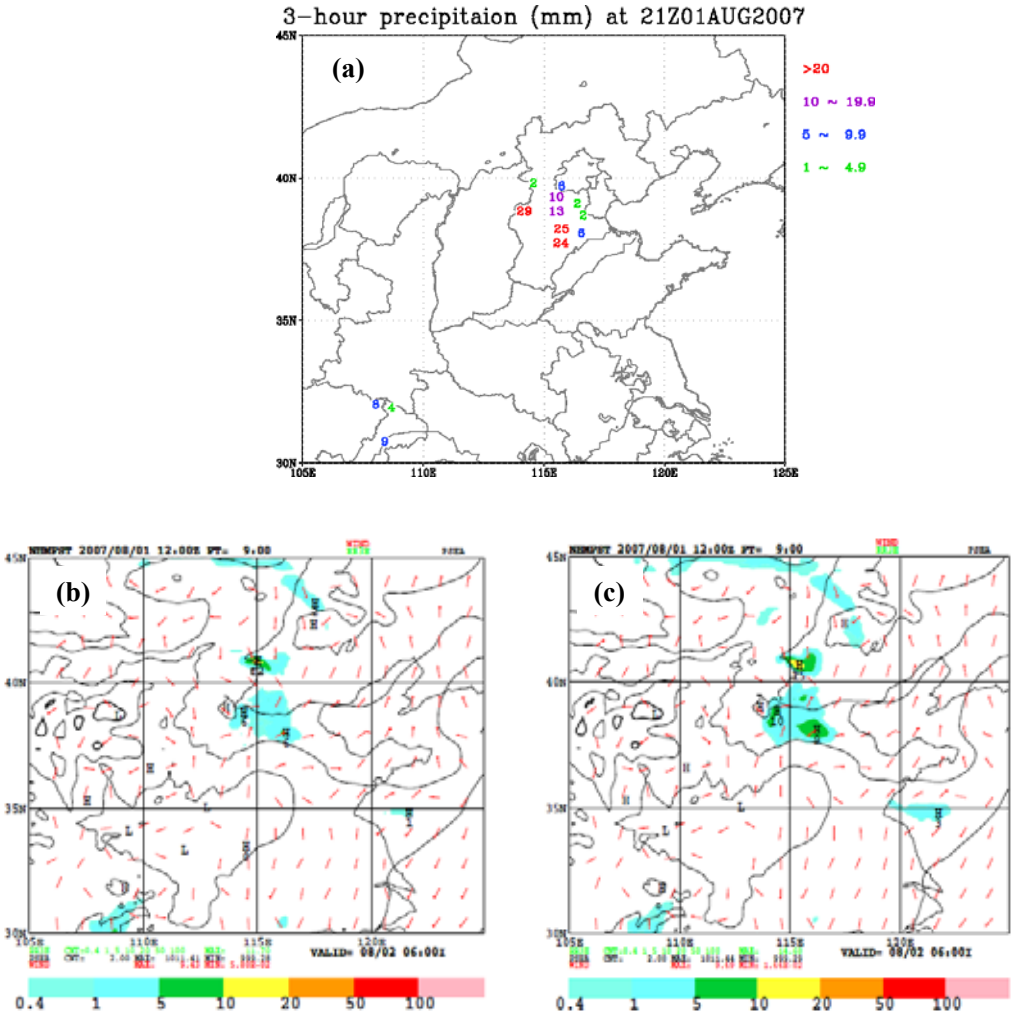

Fig. E-2-1. Accumulated 3 hour precipitation at 21 UTC 1 August 2007. **a)** Observation. **b)** Predicted rainfall by the 15 km NHM with old parameters in the K-F scheme. Initial time is 12 UTC 1 August 2007. **c)** Same as in b) but new parameters in the K-F scheme.

The bias and threat scores for 7 days from 25 July to 6 August 2008 by old and new parameters are given in Figs. E-2-2 and E-2-3. With the new parameter setting (blue lines), underestimation of weak to moderate convective rains found in the 2007 setting (red lines) was ameliorated, and threat scores were improved.

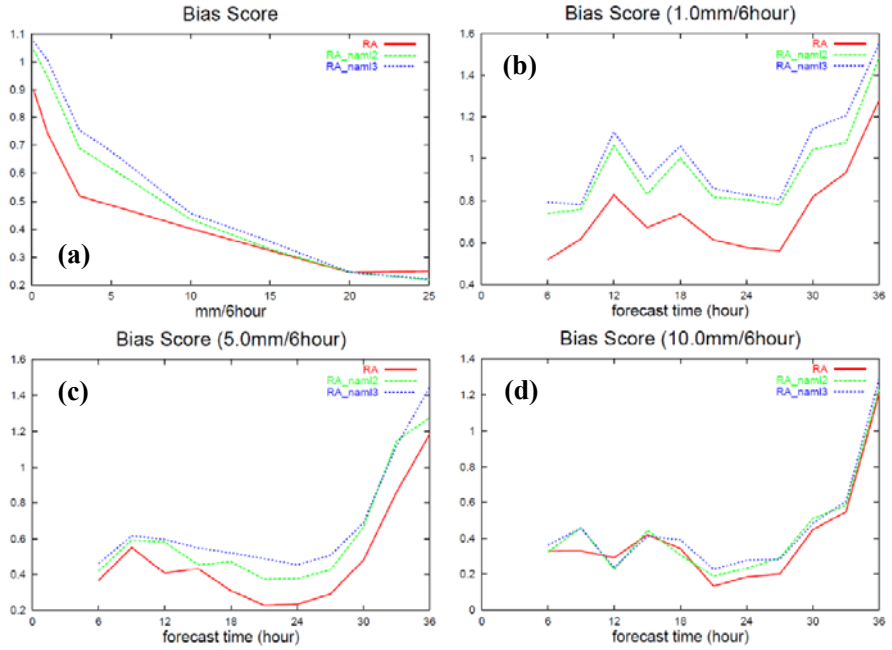

Fig. E-2-2. a) Bias scores of 6 hour precipitation against rainfall intensity for 7 days from 25 July to 6 August 2008 by old and new parameters. **b)** Time sequence of bias scores of 6 hour precipitation for weak rain (1 mm/6 hours). **c)** Same as in b) but bias scores for moderate rain (5 mm/6 hours). **d)** Same as in b) but for intense rain (10 mm/6 hours). Red lines (RA) show results by the 2007 setting, while green lines (RA_naml2) the parameters for the 10 km NHM and blue lines (RA_naml3) show results with the new parameter setting with a smaller value of kf_thresh (0.6 g/Kg).

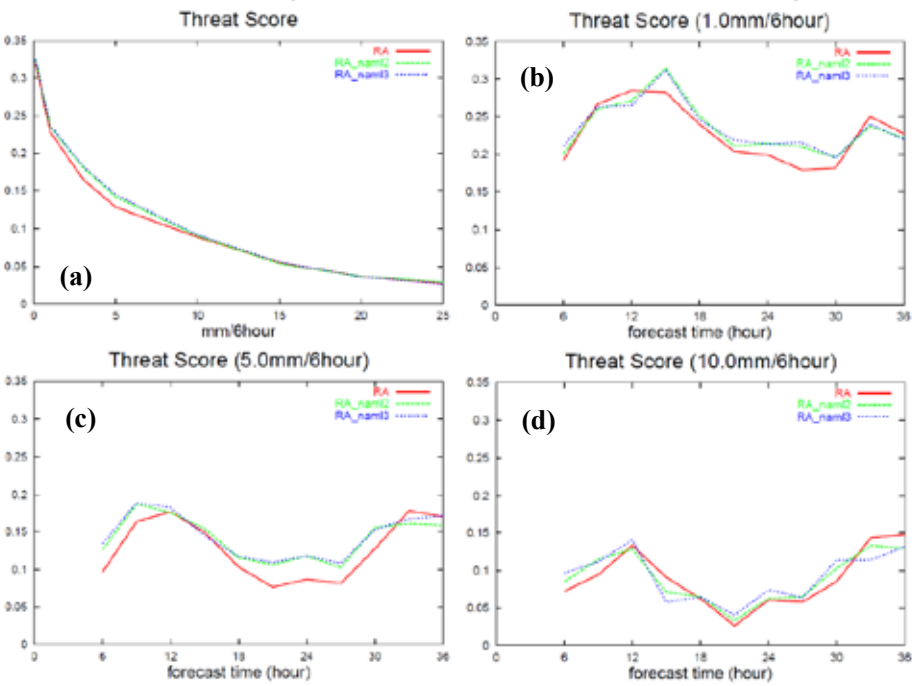

Fig. E-2-3. Same as in Fig. E-2-2 but threat scores.

E-2-2. The revision of predicting soil wetness

The soil moisture is directly related to the evaluation of the latent heat flux from the surface. If the soil is wetter, more water evaporates at the surface and more water vapor is provided to the atmosphere. The evaporation efficiency β in the parameterized latent heat flux in Eq. (F-4-14) is exactly representing this effect, and associated to the volume fraction of soil moisture with the very simple relation given as Eq. (F-4-16). The volume fraction of soil moisture is a prognostic variable in the model, which is predicted by the force-restore method. The details of the method are described in F-4.

In August 2007, extremely hot temperature such as over 38°C was sometimes observed in Japan, but the operational meso scale model that employs NHM failed to predict the high temperature. For example, Figure E-2-4 shows time series of predicted screen level temperature (with the corresponding observation), surface skin temperature, sensible and latent heat flux from the surface and evaporation efficiency at the surface at Kumagaya City on 15 August 2007. The situation of Kumagaya City is similar to that of Beijing because Kumagaya is located inland and relatively urbanized like Beijing. On

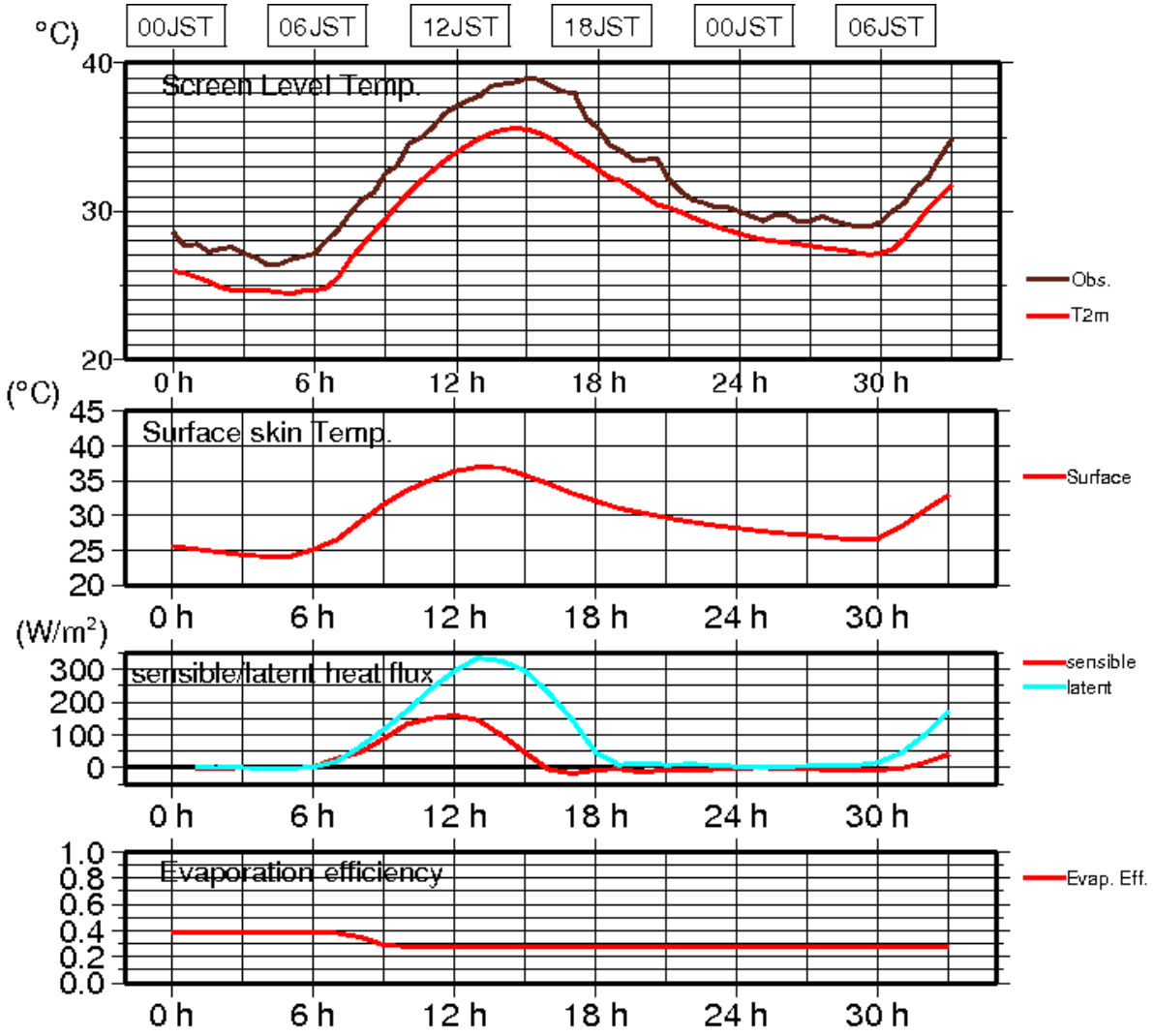

Fig. E-2-4. Time series of (from upper) screen level temperature at the height of 2m above surface with the observation, surface skin temperature, sensible and latent heat flux from the surface, and evaporation efficiency at the surface at Kumagaya city by the operational meso scale model (MSM) at JMA with the initial condition at 15UTC on 14th (00JST on 15th) August 2007.

that day, the observed screen level temperature reached almost nearly 40 ° C there, but the operational models gave only 36 ° C. The Bowen ratio in this case is about 0.28, while the typical value of it in urbanized area is said to be between 0.7 and 1. It implies that latent heat flux, the predicted peak of which is more than 300 W/m ^{2} can be far too much.

One can also find it in Figure E-2-4 that the evaporation efficiency slightly changed only at the beginning of the forecast, and kept almost constant until the end. It is because the minimum limit for the volume fraction of soil moisture was applied as mentioned in F-4. The minimum limit is implemented to be $F_{\min} w_{\text{ini}}$, where w_{ini} is the initial condition of the volume fraction of soil moisture and $F_{\min}$ is certain factor less than 1, in order to prevent the volume fraction from varying to extremely small value. On the other hand, too large $F_{\min}$ can result in excessive latent heat flux and failure of predicting extremely high temperature. The too large evaporation efficiency brought by the too strict minimum limit for soil moisture is one possible reason of the failure.

Figure E-2-5 shows predicted screen level temperature by the models with $F_{\min} = 0.7$, 0.5 and 0.4 on the day when temperature over 38 ° C was broadly observed around Beijing, telling us the sensitivity to the factor $F_{\min}$. While the model with the original value (0.7) displays too small area

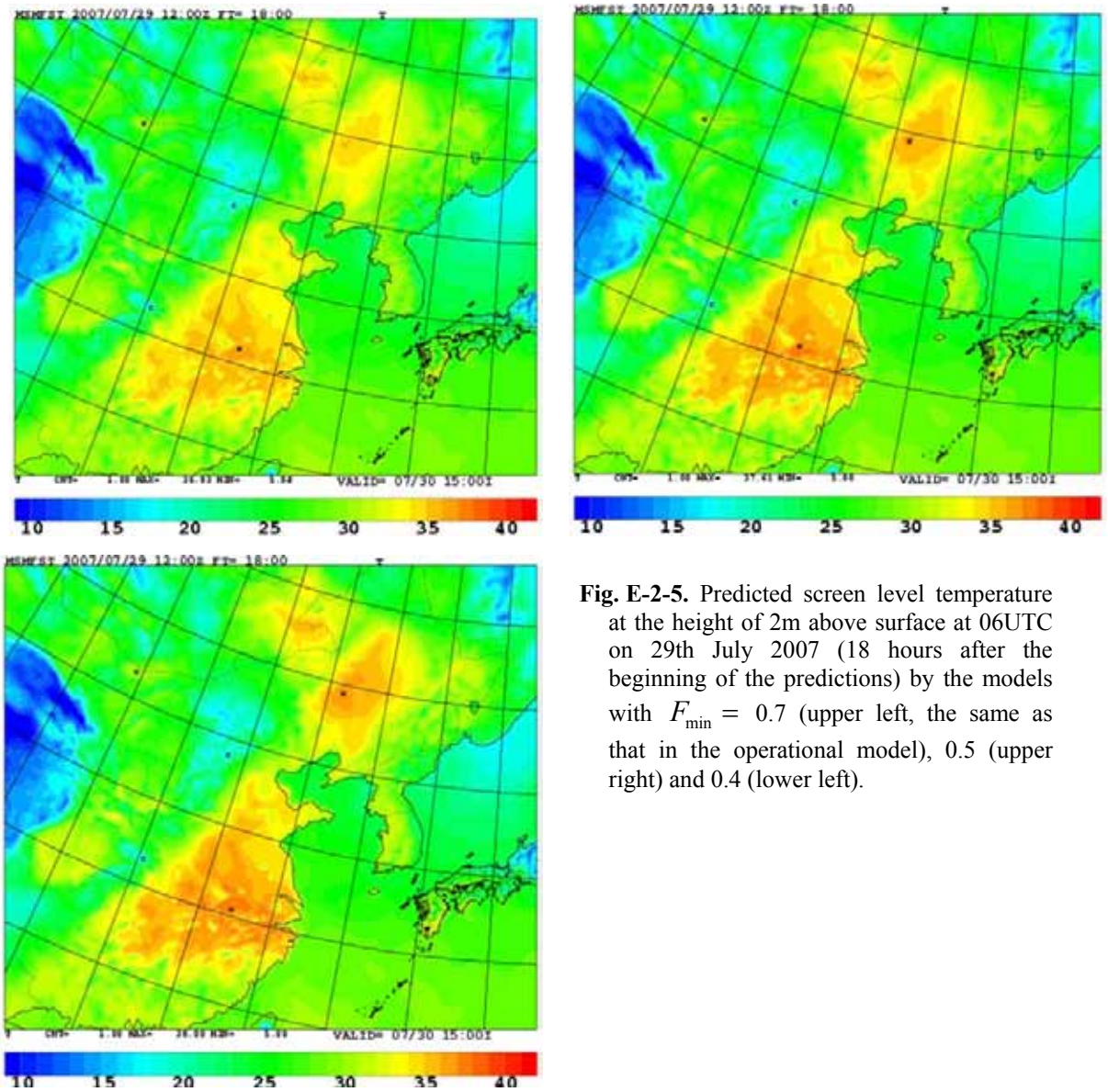

Fig. E-2-5. Predicted screen level temperature at the height of 2m above surface at 06UTC on 29th July 2007 (18 hours after the beginning of the predictions) by the models with $F_{\min}$ = 0.7 (upper left, the same as that in the operational model), 0.5 (upper right) and 0.4 (lower left).

with over 38 °C, smaller $F_{\min}$ gives the larger one as expected. The effect is dominant especially in the area where relatively high temperature was predicted even with the original value. In other words, it does not increase the temperature uniformly but increase it where high temperature should be predicted. Although it is quite simple, changing $F_{\min}$ to a smaller one has possibility to improve prediction of screen level temperature, in particular in the area where extremely high temperature is often observed such as Beijing.

In order to determine which value of $F_{\min}$ is the most suitable in this frame, some experiments were conducted with the similar configuration of the B08RDP including the domain, forecast period (36 hours), and initial time (1200UTC, or 2000LST). The experiments were carried out with the eight initial conditions through 29 July to 5 August in 2007 when extremely hot temperature were often observed around Beijing. As $F_{\min}$, 0.6 and 0.5 were chosen to be tested as well as 0.7 which is used in the operational meso scale model.

Figure E-2-6 shows the threat and bias scores to predict 2m temperature over certain thresholds at 18 hours from the beginning of the simulation, when maximum temperature can be often observed. As expected, the smaller value of $F_{\min}$ makes prediction of higher temperature more frequent, and $F_{\min} = 0.5$ is the most suitable in terms of these scores. However, the time series of mean error (ME) and root mean square error (RMSE) of 2 m temperature shown in Figure E-2-7 tells that the model with $F_{\min} = 0.5$ gives slightly too high temperature and makes RMSE worse than the control ($F_{\min} = 0.7$). On the other hand, the model with $F_{\min} = 0.6$ reduces RMSE or keeps it almost unchanged.

Figure E-2-8 reveals more serious problem with the smaller value of $F_{\min}$. It shows the time series of ME and RMSE of 2m dew points. Although the dew point at the surface had been drier even at the beginning of the forecast, the dry bias was expanded at the daytime and smaller $F_{\min}$ expanded it more. The operational value $F_{\min}$ gave the best result in terms of RMSE. It is very natural that the surface becomes drier when latent heat flux is reduced, but it is a serious problem because the surface is drier than actual even with the original value and the problem cannot be resolved only with revision of the surface process.

Taking the results above into account, $F_{\min} = 0.6$ was eventually adopted for the B08RDP through the consideration that the value can make forecast of temperature more accurate in particular for very hot cases, and the expansion of the dry bias is acceptable. Moreover, the importance of predicting extremely hot temperature around Beijing in the B08RDP encouraged us the revision.

With the revise, screen level temperature by MRI/JMA performed very well in the B08RDP. However, the experiments indicate that too much latent heat flux partly compensates the dry bias at the surface caused by other processes: the initial conditions give drier surface than actual, and the boundary layer and surface processes do not represent sufficient diurnal changes of temperature and humidity near the surface. It is no matter of course that further improvement of the surface process is necessary such as introducing a land model considering vegetation and interactions between canopy, surface skin, and atmosphere instead of the current simple slab model, but there might be some other processes to be revised in order to obtain more accurate surface temperature and humidity which is very important especially for the operational use.

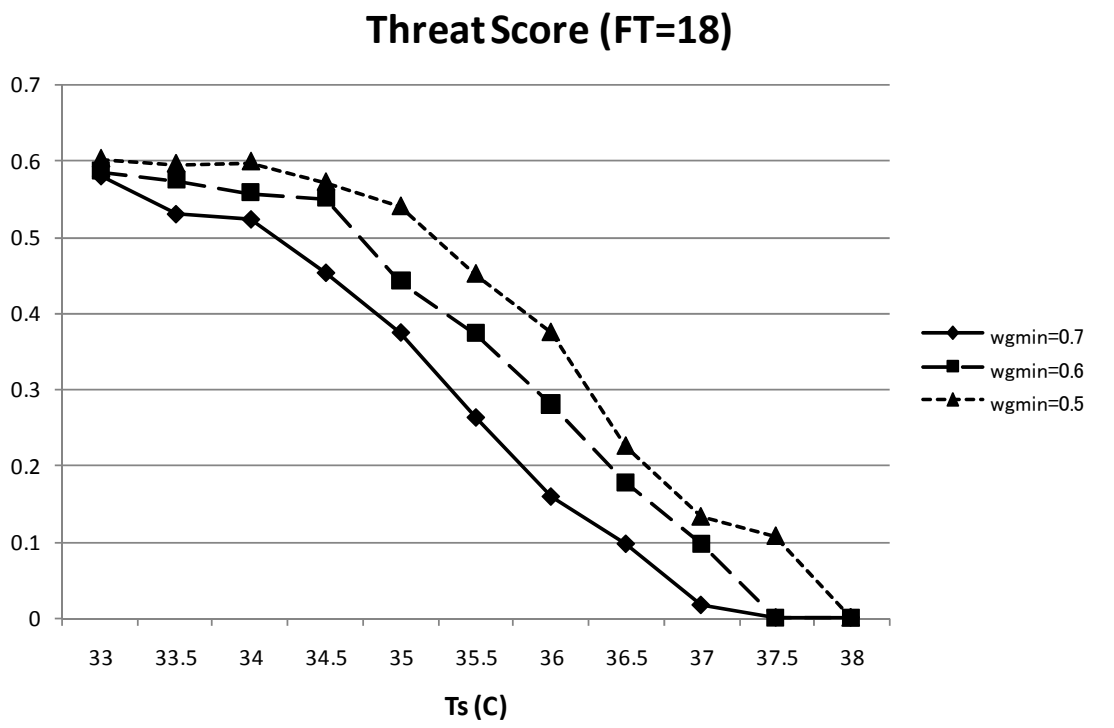

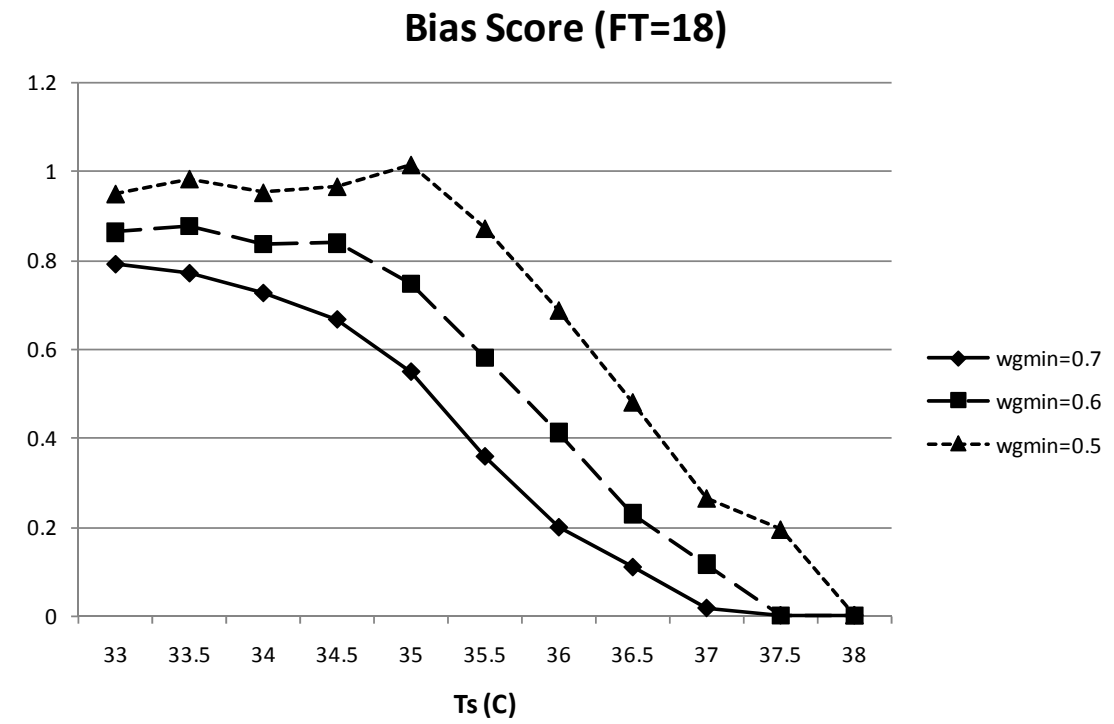

Fig. E-2-6. Threat (top) and bias (bottom) scores to predict 2m temperature over thresholds indicated at the horizontal axis by the models with three different $F_{\min}$ (denoted as "wgmin" in the figure) . Forecasts at 18 hours from the initial conditions are verified against the corresponding observations.

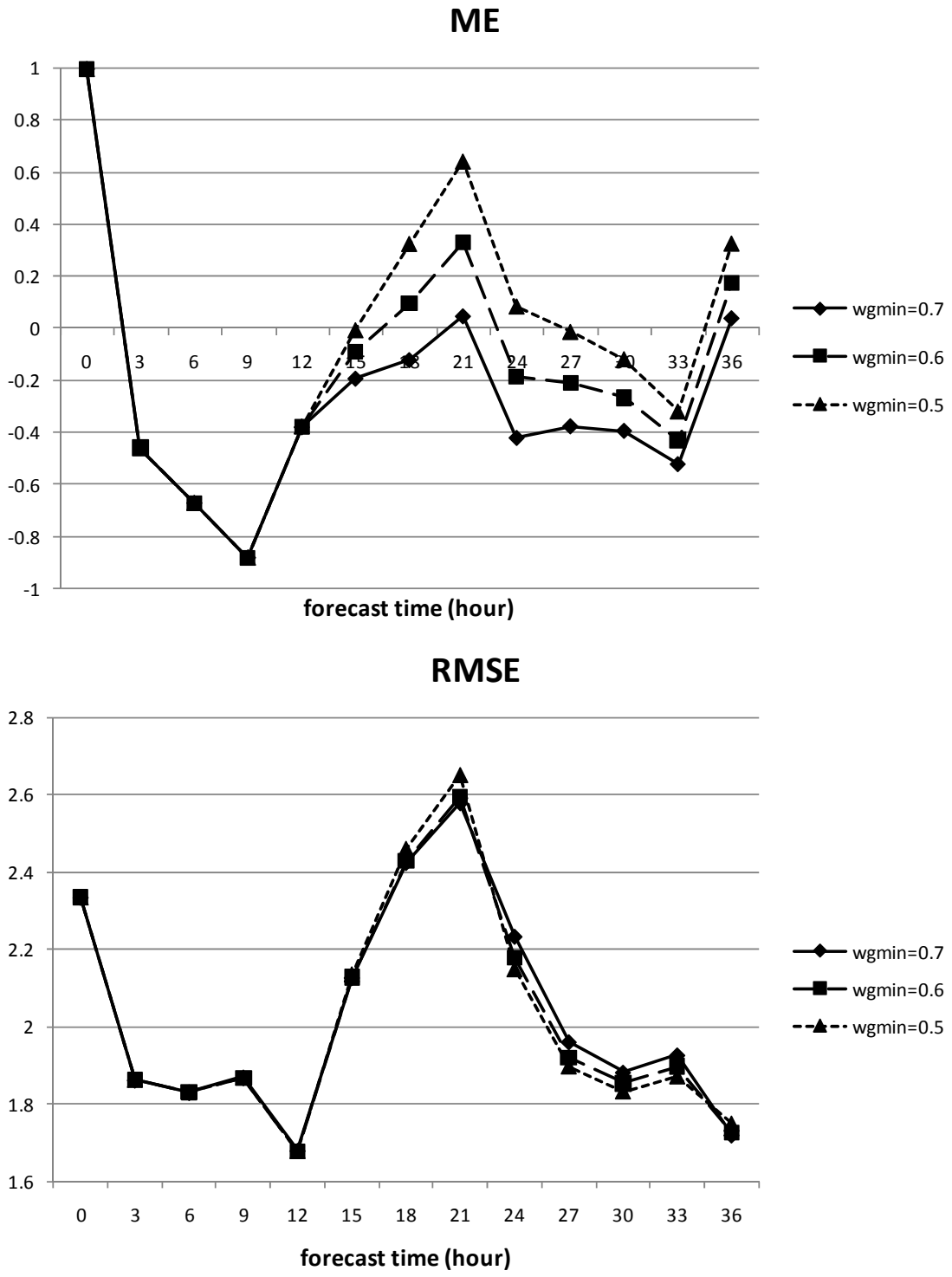

Fig. E-2-7. Time series of mean error (ME) and root mean square error (RMSE) of 2m temperature against the corresponding observation. The horizontal axis denotes hours from the initial conditions.

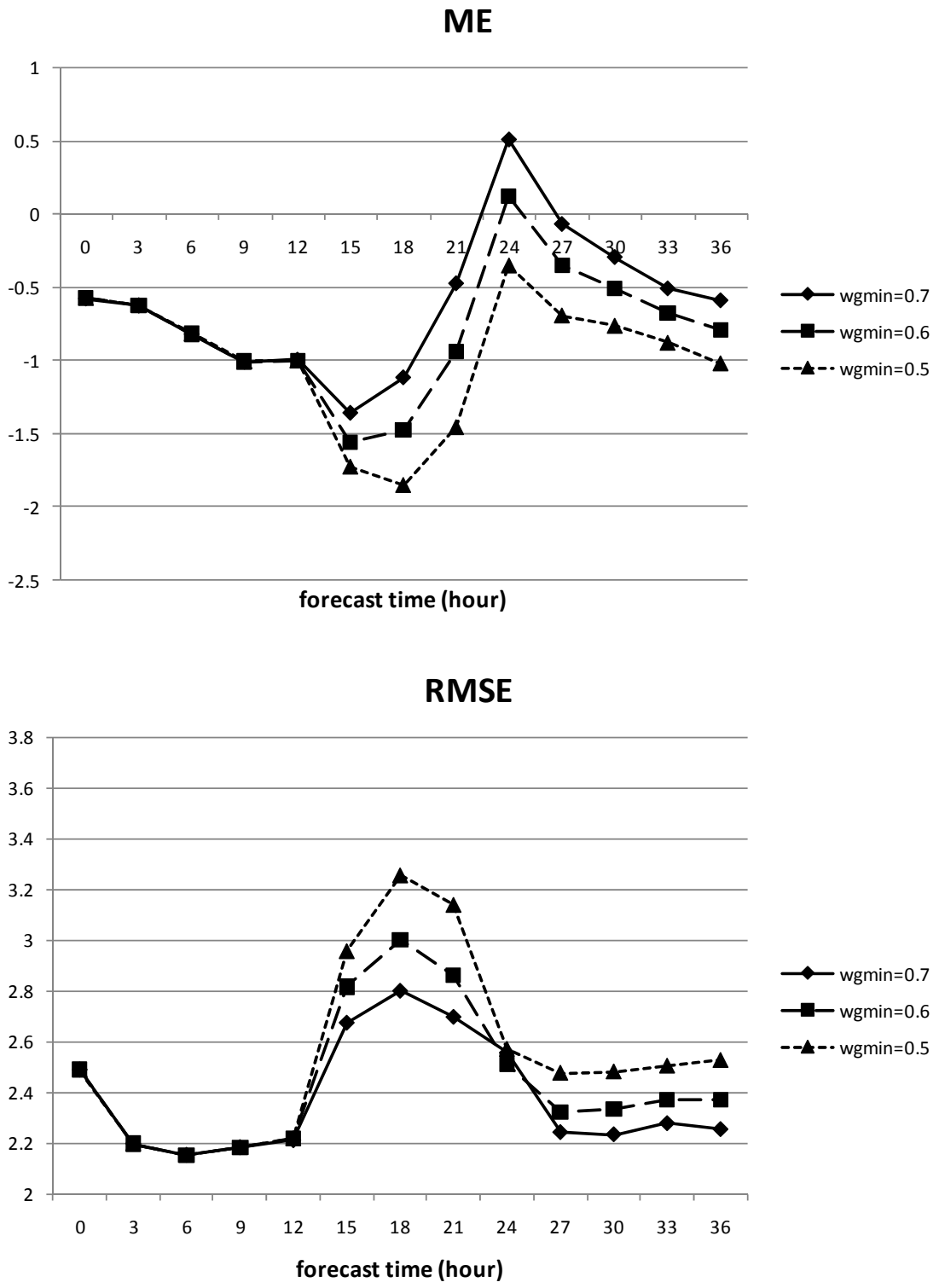

Fig. E-2-8. Time series of mean error (ME) and root mean square error (RMSE) of 2m dew point against the corresponding observation. Tested values of $F_{\min}$ are the same as Fig. E-2-4.

E-2-3. Numerical diffusion and other parameters

In addition to the tuning of parameters in the K-F convective parameterization, auto-conversion rates from cloud to rain (autr2) and to snow (auts2) in cloud microphysics, threshold values and the 1/e folding time in the targeted moisture diffusion (TMD; Saito and Ishida, 2005), and parameters for numerical diffusion are adjusted to ameliorate the underestimation of precipitation and to improve computational robustness in the simulation with a horizontal resolution of 15 km. Parameters used in the B08RDP experiments and operational MSM are listed in Table E-2-1. Most parameters in the 2008 experiment are the same values as in the operational 10km MSM, except that the 1/e folding time of nonlinear computational diffusion was changed from 2400 s to 1500 s.

Table E-2-2. Parameters used in the B08RDP experiments and operation MSM.

	Name of variable	Operational NWP (MSM5kmL50)	Operational NWP (MSM10kmL40)	B08RDP (2006)	B08RDP (2007)	B08RDP (2008)
Time step	**DT**	24	40	60	60	60
KF scheme						
Threshold for conversion of condensation to rain	kf_thresh	2.00x10-3	0.80x10-3	0.80x10-3	2.00x10-3	0.60x10-3
Life time of deep convection	cu_lifetime	900	1800	1800	900	1800
Life time of shallow convection	shallow_lifetime	600	2400	2400	600	2400
Cloud microphysics						
Auto-conversion rates from cloud to rain and snow	autr2, auts2	10^{-3}	10^{-4}	10^{-4}	10^{-3}	10^{-4}
Targeted moisture diffusion (TMD)						
Threshold to apply TMD (m/s) 1/e folding time (sec)	wthrt, diftg	3.0, 300	2.0 , 300	2.0 , 300	2.0 , 300	2.0, 300
Numerical diffusion 1/e folding time (sec)						
Non linear diffusion 4th order diffusion Boundary and lateral Rayleigh damping	difnl, dif2d rldmpx, rldmpz	1200*, 600 2400	2400, 1200 2400	2400, 1200 2400	2400, 1200 2400	1500, 1200 2400

* changed to -600 after 17 September 2008.

E-2-4. Adoption of the generalized vertical hybrid coordinates

The generalized vertical hybrid coordinates has been implemented in the operational MSM since May 2007, whereas not the new vertical hybrid coordinates but the terrain-following coordinates

$$z^* = \frac{H(z - z_s)}{H - z_s}, \tag{E-2-1}$$

were used in the 2007 B08RDP preliminary experiment due to the consistency in the initial perturbation methods. In the 2008 experiment, the new vertical hybrid coordinates were employed for initial and boundary perturbation methods and the 36 hour extended ensemble forecast. The generalized vertical hybrid coordinates of NHM (Ishida, 2007) is given by

$$\zeta = z - z_s f(\zeta), \tag{E-2-2}$$

$$f(\zeta) = \frac{c\{1 - (\frac{\zeta}{z_T})^n\}}{c + (\frac{\zeta}{z_T})^n}, \tag{E-2-3}$$

where z_s is the surface height of orography, z_T is model top height and n=3 is used. Coefficient c in (E-2-3) is defined by

$$c = \frac{(\frac{z_l + z_h}{2z_T})^n}{1 - 2(\frac{z_l + z_h}{2z_T})^n}, \tag{E-2-4}$$

where z_l and z_h are the heights which define the transition of hybrid coordinates' characteristics; above z_h the model plane becomes flat and below z_l the model plane becomes almost parallel to the terrain surface. In the 2008 B08RDP experiment, values of z_l =1000 m and z_h =11,000 m were used for 40 levels NHM (z_T =22 km).

E-3. Initial and boundary conditions

In the B08RDP experiment, initial conditions for the MEP system needed to be prepared by each participant. Needless to say, the accuracy of the analysis field is essential for MEP because it can be regarded as the center of the probability density function of the initial states.

Since JMA terminated regional analysis in November 2007, only the JMA global analysis (GA) was available for near-real-time experiments over the full domain of B08RDP as of Summer 2008. However, the horizontal resolution of the inner model of global 4D-Var in GA (T159; about 80 km) was not fine enough for mesoscale numerical predictions. There are also distinct disparities between GA and the subsequent mesoscale model, such as the land-surface processes, which would make it difficult to execute the model forecast.

In order to assimilate the observational data with high resolution and to produce more accurate initial fields than GA, the JMA mesoscale 4D-Var analysis system (Meso 4D-Var), which was originally designed to cover the area around Japan, was modified so as to permit its use in the China area. In addition to conventional observational data, precipitation data observed by rain gauges in China were assimilated by the Meso 4D-Var. Moreover, we tested the impact of the precipitation analysis performed by the Australian Bureau of Meteorology in FDP (Seed 2009). These trials were carried out following the work of Koizumi et al. (2005), which examined the impact of the assimilation of a rainfall analysis produced by a nowcasting project.

E-3-1. Application of Meso 4D-VAR

The Meso 4D-Var analysis system (Ishikawa and Koizumi 2002) was developed based on the JMA hydrostatic mesoscale spectral model. Since the original domain (3600 km × 2880 km) covered only Japan and its surrounding areas, we shifted and expanded the domain to fully cover the common verification region of B08RDP with the margins at the lateral boundaries (Fig. E-3-1). The domain size was 3600 km × 3200 km, and the number of vertical levels was 40, from the surface up to 10 hPa. An incremental method was used for the iteration procedure in the 4D-Var system to enhance the computation efficiency. The inner model had a 20 km horizontal resolution, which was coarser than that of the outer model, at 10 km.

In the JMA data-assimilation systems, the background error statistics are calculated using the NMC (National Meteorological Center, later National Centers for Environmental Prediction (NCEP)) method (Parrish and Derber 1992). Strictly speaking, if the model domain is changed, the background error statistics should be re-calculated. In this study, the same statistics as in the original 4D-Var were used for simplicity, based on the assumption that the statistics over East Asia are not significantly different.

The assimilation window length was 3 hours, with the observational data collected into four 1-hour time slots. Typical observational data are obtained from radiosondes, land stations, pilot balloons, wind profilers, aircrafts, ships, and buoys. In addition to these conventional data, the JMA's Radar-Raingauge analyzed precipitation (estimated by weather radars and calibrated by ground-based rain gauges) over Japan and satellite-retrieved data from the Special Sensor Microwave/Imager (SSM/I), The Tropical Rainfall Measuring Mission Microwave Imager (TMI) and the Advanced Microwave Scanning Radiometer for Earth Observing System (AMSR-E) were assimilated as a 1-hour

precipitation amount or as total precipitable water (TPW). QuikSCAT sea-surface winds and radial velocity data for operational Doppler radars in Japan were also assimilated. These features are summarized in Table E-3-1.

In the B08RDP experiment, all participants operated their MEP systems once a day, initialized at 1200 UTC, for up to 36 hours. Considering the computational resources, we arranged for the data assimilation cycle to be conducted over just 6 hours, from 0600 UTC to 1200 UTC, without a continuous analysis-forecast cycle. To reduce the discrepancy factors between the analysis model (20 km hydrostatic model) and the forecast model (15 km NHM), the incremental forecast in the second assimilation window (0900 to 1200 UTC) was performed using the 15 km NHM. For better understanding of the experimental setup, a schematic diagram of the assimilation experiment and the subsequent model forecast is shown in Fig. E-3-2. Using the forecast of the 15 km NHM for analysis fields, the cloud microphysical variables (cloud water, cloud ice, rain, and graupel) at 1200 UTC were given at the initial time of MEP. This method effectively avoids underestimation of the precipitation in the spin-up period (Ishida and Saito, 2005). A similar method has been employed in the JMA operational mesoscale forecast (Aranami and Hara, 2006).

In order to utilize as much observational data as possible in the assimilation cycle, the system was employed after waiting for the arrival of radiosonde data in China at 1200 UTC. These data have a time lag of a few hours and are not assimilated in the operational mesoscale analysis at JMA. Since the B08RDP participants were requested to send the MEP results to CMA by 2230 UTC, this waiting time could constrain the schedule for subsequent job steps, such as ensemble forecasting. However, preliminary experiments indicated that the forecast accuracy was clearly degraded if the upper soundings over China at 1200 UTC were not assimilated (Fig. E-3-3).

E-3-2. Assimilation of rain observation

Although the satellite data are assimilated as retrieved water vapor and precipitation data in the Meso 4D-Var, they seemed to have little impact on predicting precipitation over China because the data are limited over the sea, located southeast of the model domain. Hence, in this study, 3-hour rainfall amounts observed by rain gauges in China and 1-hour rainfall analysis data from around the Beijing area (STEPS: Short-Term Ensemble Prediction System) were assimilated complementarily.

The STEPS data were obtained from the B08FDP component, in which the Australian Bureau of Meteorology (BOM) routinely produced data for their nowcasting system during the FDP experiment period. STEPS is a quantitative precipitation estimate (QPE) system at BOM that blends hourly rain-gauge rainfall with hourly radar rainfall (Bowler et al., 2006). In the B08FDP, some modifications were implemented, such as the alternation of the radar reflectivity factor (Z) and the rainfall rate (R) relation (Z-R relation), and the adoption of radar quality-control algorithms (Seed, 2009). Although the data covered only a domain of 500 km square around Beijing (Fig. E-3-4b), the horizontal resolution of 2 km was sufficient to be assimilated in Meso 4D-Var.

These precipitation data were processed by averaging and interpolating them into the 20 km inner grids of Meso 4D-Var and were assimilated following Koizumi et al. (2005). Since we discarded any precipitation data of less than 0.5mm/hour, no-rain information was not used in the assimilation process. This procedure was introduced because it was impossible to distinguish between a null report and no rain in the 3-hour accumulated rain-gauge data provided by CMA.

Figure E-3-4a (E-3-4b) indicates the distribution of 3-hour accumulated rainfall observed by rain gauge (analyzed by STEPS). Figures E-3-4c and E-3-4d present the corresponding rainfall in the analysis cycle of the Meso 4D-Var system. The rainfall around the Beijing area is weak in the experiment without precipitation-data assimilation (MA; Fig. E-3-4c) compared with the rain-gauge observations (Fig. E-3-4a). By contrast, the experiment with precipitation-data assimilation (MA_CRAIN) successfully captures the features of the distribution of observed rainfall around the Beijing area (Fig. E-3-4d). This result demonstrates that these rainfall data were assimilated properly.

E-3-3. Soil temperatures

In the first window of the 4D-Var, GA was used as the initial condition at 06 UTC because we didn't adopt the successive data assimilation cycle. Because the land process of the JMA global model was different from that of the Meso 4D-Var as well as NHM, a special treatment was required regarding the soil temperatures at the beginning of the assimilation cycle. That is, in the JMA global model, the Simple Biosphere scheme (SiB) has been implemented where 1-layer deep soil temperature is predicted with the force restore method. On the other hand, 4-layer soil temperatures are predicted using the heat conduction equation in NHM and the Meso 4D-Var.

To prepare the initial soil temperatures (denoted by 'tin') in Meso 4D-Var at 06 UTC, the ground surface temperature of the global analysis was substituted for the first layer soil temperature of the mesoscale model ($\mathrm{tin}(1)$). Soil temperatures at other layers ($\mathrm{tin}(2)$, $\mathrm{tin}(3)$, $\mathrm{tin}(4)$) were given by climatological values calculated from the Japanese 25-year Reanalysis Project (JRA-25; Onogi et al. 2007). The climatological soil temperatures were calculated by flowing equation (JMA 2007, Aranami 2007; personal communication, Hara 2008):

$$\mathrm{tin(i)} = \hat{\mathrm{T}} + \mathrm{A}\exp\left(-\frac{\mathrm{z_i}}{\mathrm{d}}\right)\cos\left\{\frac{2\pi}{365}(\mathrm{D}-\mathrm{P})-\frac{\mathrm{z_i}}{\mathrm{d}}\right\}, \qquad \text{(E-3-1)}$$

where $\hat{\mathrm{T}}$ is the mean soil temperature calculated from the JRA-25, A and P are the amplitude and the phase of the annual component of the surface temperature, respectively, $\mathrm{z_i}$ is the depth of the i-th ground layer and d (=2.65m) is the e-folding depth and D is the number of day from the beginning of the year.

To take into account the influence of the diurnal change at the surface layer on the lower layers, $\mathrm{tin}(2)$ was further modified using $\mathrm{tin}(1)$ as follows:

$$\mathrm{tin}(2) = \mathrm{tin}(2) + (\mathrm{tin}(1) - \mathrm{tin}(2))\exp(-\mathrm{z_2}/\mathrm{d_2}), \qquad \text{(E-3-2)}$$

where $\mathrm{z_2}$ is the depth of the second layer (=0.115 m) and $\mathrm{d_2}$ is the depth where the amplitude of the surface temperature become 1/e in the diurnal cycle (=0.140 m).

Above method developed for the B08RDP has been implemented in NHM, and is applicable to forecast experiments using GA.

E-3-4. Verification of control forecasts in MRI/JMA

In the experiment conducted during the 2008 summer season, we verified the performance of the control forecasts of the MRI/JMA MEP system using threat and bias scores from 6-hour accumulated precipitation. In the final experiment of B08RDP, we adopted the Meso 4D-Var analysis with precipitation assimilation (MA_CRAIN) to prepare the initial conditions for the control run. For

comparison, additional experiments were performed after the final experiment using Meso 4D-Var without assimilation of precipitation data in China (MA) and the JMA global analysis (GA). Although the MA experiment was not carried out in real time, the assimilated observations were the same as in the MA_CRAIN experiment, especially the upper soundings at 1200 UTC. The GA experiment was performed for comparison, using MA and MA_CRAIN as a reference. GA is produced by the JMA global 4D-Var with a horizontal resolution of about 80 km. The assimilation length is 6 hours, with observational data taken within 3 hours before and after analysis time being assimilated. For details, see JMA (2007).

Figure E-3-5 compares threat scores, and Fig. E-3-6 compares bias scores, both averaged from 25 July to 23 August 2008. For threat scores against the intensity of precipitation (Fig. E-3-5a), we can see that the Meso 4D-Var results were superior to GA at almost all thresholds. With precipitation assimilation, the scores were further improved, particularly for weak and moderate rains (Figs. E-3-5b and E-3-5c). For the bias scores, precipitation assimilation also contributed to the improvement of the scores for weak and moderate rains (Fig. E-3-6a), though the effect becomes unclear in the latter half of the forecast period. The most notable characteristic is that the bias scores of MA_CRAIN and MA at the beginning of the forecast period (Figs. E-3-6b, E-3-6c, and E-3-6d) are considerably better than those of GA. Implementing NHM in the outer model of the 4D-Var partly contributed to improving the model spin-up.

It is also important to examine the error statistics of other variables when evaluating the validity of the precipitation assimilation. Figure E-3-7 presents the time series of the mean error (ME) and root mean square error (RMSE) for the surface temperature and relative humidity, averaged over the experiment period. For the surface temperature (Figs. E-3-7a and E-3-7b), we can see that the negative bias of MA_CRAIN was slightly larger at the beginning of the forecast period than that of MA, whereas the RMSEs were almost identical. This seems attributable to the fact that the assimilation of rainfall rates mostly enhanced the precipitation in analysis cycles, leading to a lowered surface temperature through the evaporation of raindrops and advection of cold air. For the relative humidity at surface level (Figs. E-3-7c and E-3-7d), the bias of MA_CRAIN was again slightly increased, highlighting the lowered temperature. However, the RMSE was not degraded. These results suggest that the assimilation of rainfall amounts has a clear advantage in precipitation forecasts and is almost neutral regarding the prediction of surface temperature and relative humidity.

Figures E-3-5 and E-3-6 indicate that MA was superior to GA for the initial condition of the mesoscale model forecast, despite the advantage of having observational data taken after the analysis time assimilated in GA. This is partly because of dry bias at the surface level (Fig. E-3-7c) caused by the difference in land processes between GA and MA mentioned above. This discrepancy yielded higher land-surface temperatures and lower relative humidity in GA than in MA, which would lead to deterioration of the precipitation forecast in the subsequent model. Although GA was used as a first guess at the beginning of the MA cycle, the 6-hour assimilation period was long enough to reduce the bias of surface temperature and relative humidity with observational data.

It should be noted that there remains a difficulty in predicting intense rainfall. We can see that the advantages of assimilating precipitation data were not so obvious for intense rainfall (Figs. E-3-5d and E-3-6d). This might be partly related to the forecast model resolution of 15 km in the B08RDP experiment, where cumulus convection was parameterized using a modified Kain-Fritsch scheme.

Another cause may be in the initial condition; Meso 4D-Var is a hydrostatic data assimilation method without cloud microphysics. The horizontal resolution of the inner model is 20 km, and the precipitation intensities were assimilated in cube-root form in order to avoid excess influence of the data.

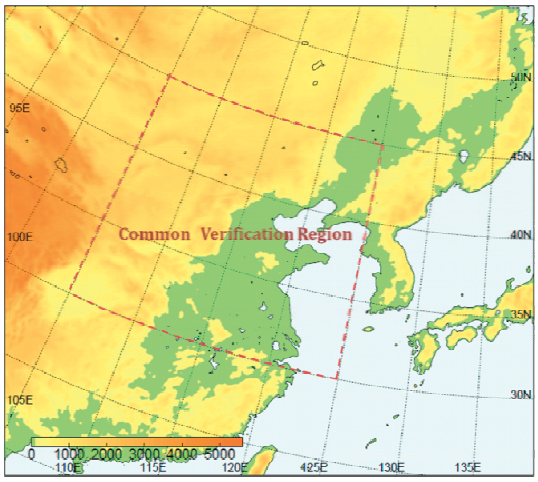

Fig. E-3-1. Domain of the Meso 4D-Var applied to B08RDP. The area surrounded by dashed lines is the common verification region of the B08RDP experiment. After Kunii et al. (2010a)

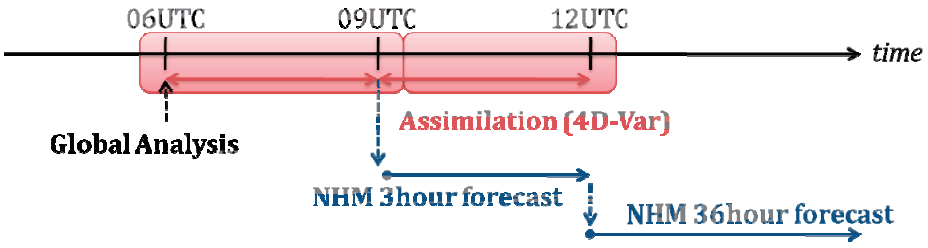

Fig. E-3-2. A schematic diagram of the assimilation experiment and subsequent model forecast.

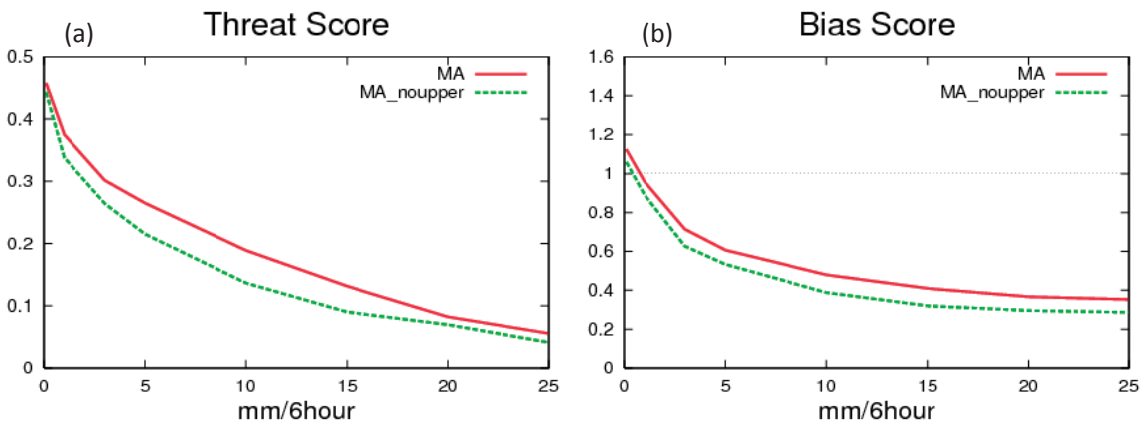

Fig. E-3-3. (a) Threat scores of 6-hour accumulated rainfall averaged for 20 to 25 June 2008; (b) same as (a) but for bias scores. MA (MA_noupper) indicates the Meso 4D-Var (Meso 4D-Var without upper soundings) over China at 1200 UTC. After Kunii et al. (2010a)

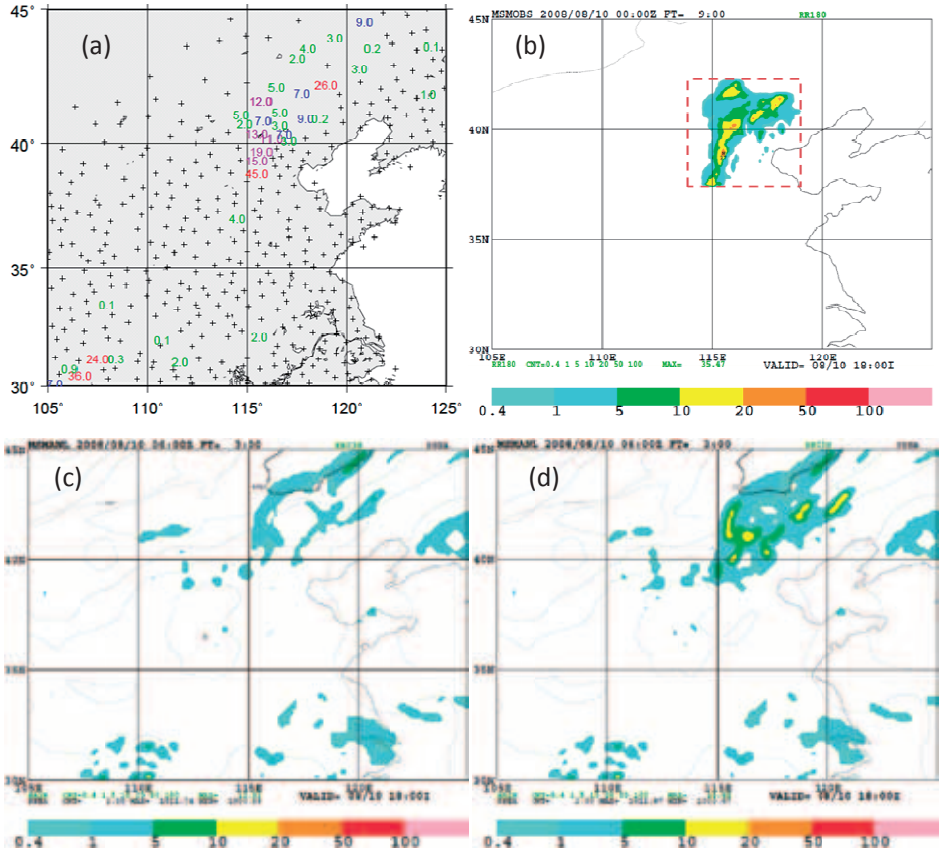

Fig. E-3-4. 3-hour accumulated rainfall on 09UTC 10 August 2008, (a) rain gauge observations, (b) Analysis by STEPS (the square surrounded by dashed lines), (c) Meso 4D-Var analysis without the precipitation data assimilation, (d) same as (c) but with the precipitation data assimilation. After Kunii et al. (2010a)

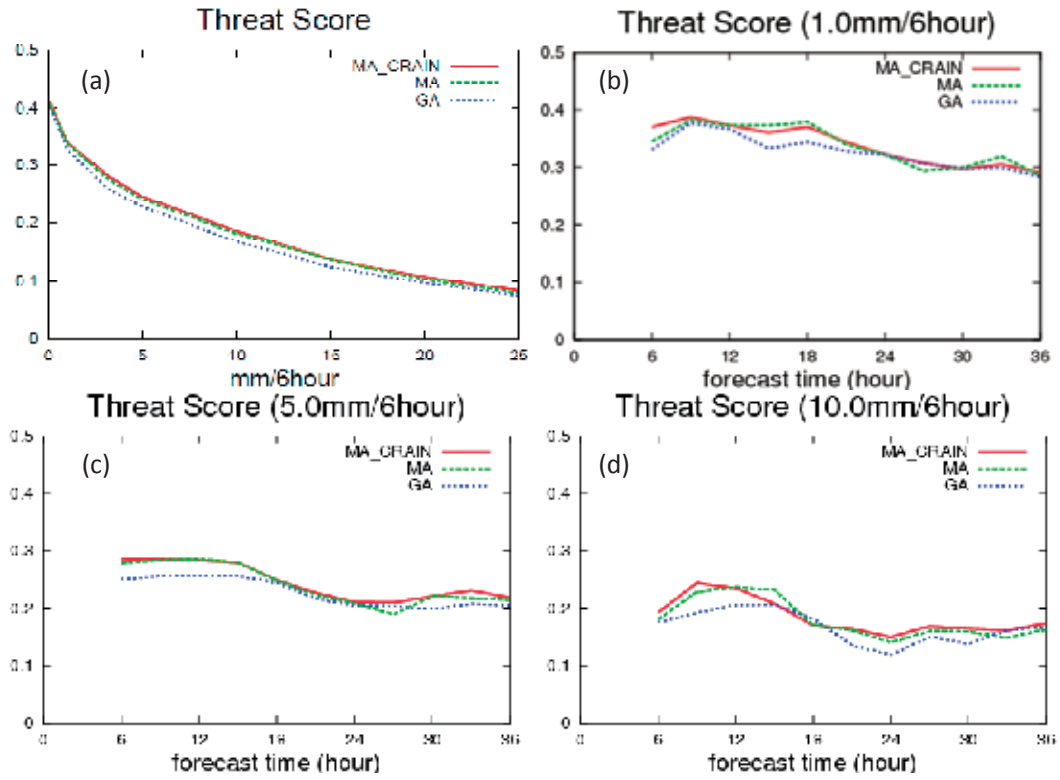

Fig. E-3-5. (a) Threat scores for 6-hour accumulated precipitation against precipitation intensity for 30 days, from 25 July to 23 August 2008. MA_CRAIN (MA) indicates forecasts from the Meso 4D-Var with (without) precipitation assimilation. GA presents forecasts from the JMA global analysis. (b) Same as (a) but time evolution of threat scores at a threshold of 1mm. (c) Same as (b) but at a threshold of 5mm. (d) Same as (b) but at a threshold of 10mm. After Kunii et al. (2010a)

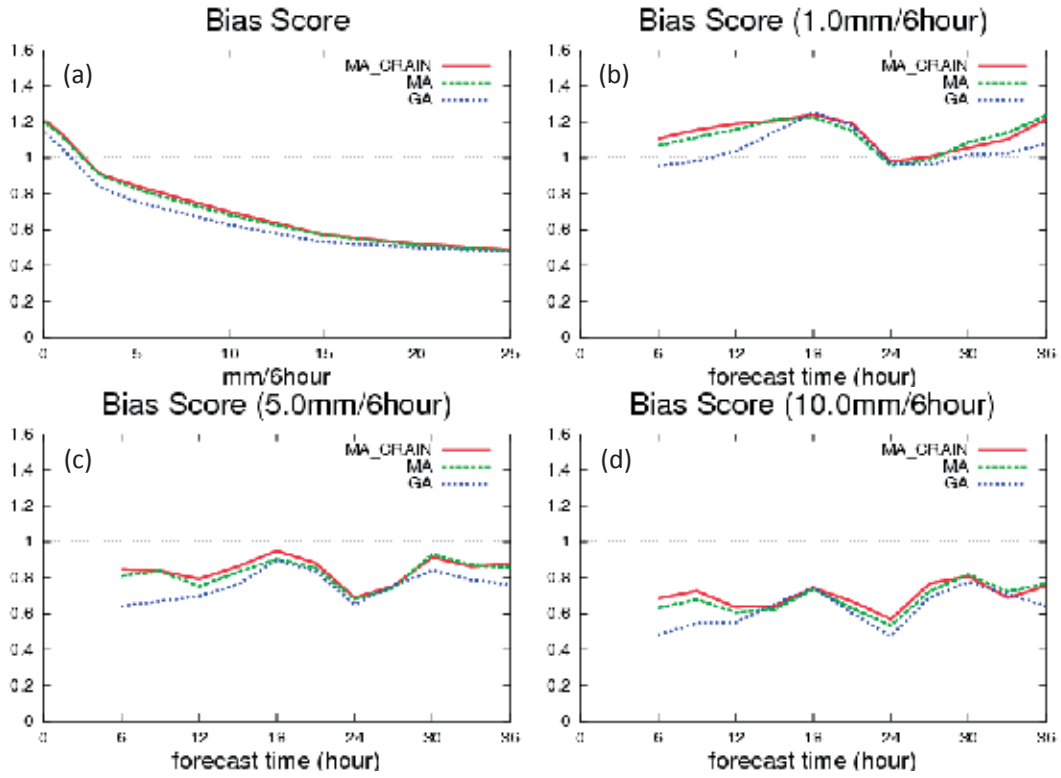

Fig. E-3-6. Same as Fig E-3-5, but bias scores. After Kunii et al. (2010a)

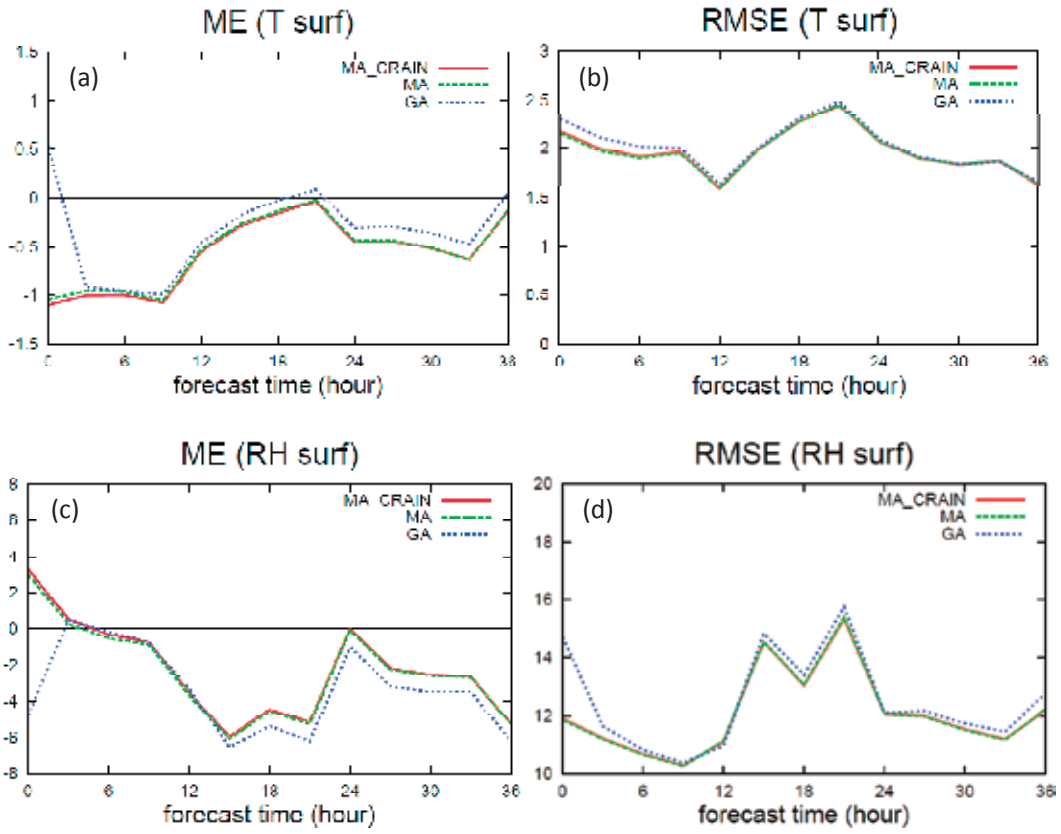

Fig. E-3-7. (a) Mean error for surface temperature. (b) Same as (a) but root-mean-square error. (c) Same as (a) but for surface relative humidity. (d) Same as (c) but root-mean-square error. After Kunii et al. (2010a)

Table E-3-1. Specifications of the Meso 4D-Var. After Kunii et al. (2010a)

Point	Description
Domain size	3600 (km) × 3200 (km)
Grid number	181 × 161 × 40
Horizontal resolution	20 (km)
Assimilation window	3 hours
Initial condition	JMA global analysis (TL959L60)
Boundary condition	JMA global forecast (TL959L60)
Observational data	radiosonde, land station, pilot balloon, wind profiler, aircraft, ship, buoy, Radar-Raingauge analyzed precipitation, precipitation amount and TPW retrieved from SSM/I, TMI and AMSR-E, QuikSCAT sea surface winds, Doppler radar radial wind.

E-3-5. Lateral boundary condition for control run

The lateral boundary condition in the 2008 experiment was given by the JMA's high resolution (TL959L60) GSM forecasts. The one-hourly data with an original model plane of the GSM at 00, 06, 12, 18 UTC were sent daily to MRI for the boundary condition of MSM (mfboundary) through the exclusive line. In order to fully cover the B08RDP model domain (Fig. D-2-1), which was shifted westward in 2007, similar but 3-hourly data at 12 UTC were prepared at JMA and were transferred to MRI daily in near real time.